Nuclear Engineering and Technology 53 (2021) 2696–2707

Contents lists available at ScienceDirect

Nuclear Engineering and Technology

journal homepage: www.elsevier.com/locate/net

Original Article

Efficiency of various structural modeling schemes on evaluating seismic performance and fragility of APR1400 containment building

Duy-Duan Nguyen [a, b], Bidhek Thusa [a], Hyosang Park [a], Md Samdani Azad [a], Tae-Hyung Lee [a, *]

[a] Department of Civil and Environmental Engineering, Konkuk University, South Korea
[b] Department of Civil Engineering, Vinh University, Viet Nam

ARTICLE INFO

Article history:
Received 6 August 2020
Received in revised form
1 February 2021
Accepted 7 February 2021
Available online 19 February 2021

Keywords:
Reactor containment building
Beam-truss element model
Multi-layer shell model
Floor response spectrum
Time-history analysis

ABSTRACT

The purpose of this study is to investigate the efficiency of various structural modeling schemes for evaluating seismic performances and fragility of the reactor containment building (RCB) structure in the advanced power reactor 1400 (APR1400) nuclear power plant (NPP). Four structural modeling schemes, i.e. lumped-mass stick model (LMSM), solid-based finite element model (Solid FEM), multi-layer shell model (MLSM), and beam-truss model (BTM), are developed to simulate the seismic behaviors of the containment structure. A full three-dimensional finite element model (full 3D FEM) is additionally constructed to verify the previous numerical models. A set of input ground motions with response spectra matching to the US NRC 1.60 design spectrum is generated to perform linear and nonlinear time-history analyses. Floor response spectra (FRS) and floor displacements are obtained at the different elevations of the structure since they are critical outputs for evaluating the seismic vulnerability of RCB and secondary components. The results show that the difference in seismic responses between linear and nonlinear analyses gets larger as an earthquake intensity increases. It is observed that the linear analysis underestimates floor displacements while it overestimates floor accelerations. Moreover, a systematic assessment of the capability and efficiency of each structural model is presented thoroughly. MLSM can be an alternative approach to a full 3D FEM, which is complicated in modeling and extremely time-consuming in dynamic analyses. Specifically, BTM is recommended as the optimal model for evaluating the nonlinear seismic performance of NPP structures. Thereafter, linear and nonlinear BTM are employed in a series of time-history analyses to develop fragility curves of RCB for different damage states. It is shown that the linear analysis underestimates the probability of damage of RCB at a given earthquake intensity when compared to the nonlinear analysis. The nonlinear analysis approach is highly suggested for assessing the vulnerability of NPP structures.

1. Introduction

The reactor containment building (RCB) is one of the most critical structures in nuclear power plants (NPPs). The recent earthquakes in South Korea such as Gyeongju (2016) and Pohang (2017) have occurred nearby NPPs, raising concerns about the safety of those structures. Therefore, it is necessary to continue studying seismic performances and fragilities of NPP structures and components. The finite element analysis method has been considered as one of the most effective approaches for simulating seismic behaviors of civil infrastructures and nuclear structures.

In particular, RCB is commonly modeled by the lumped-mass stick model (LMSM) or three-dimensional finite element model using solid elements (3D FEM). LMSM simplifies the real structures to linear-elastic beam elements with concentrated masses at nodes. This modeling approach has been widely applied for seismic response analyses and vulnerability assessments of NPP structures [1–7] and equipment [8–10]. Some studies improved the accuracy of LMSM by using the frequency adaptive technique and modal characteristics of structures [10,11]. While the simplicity of the modeling and the calculation are the advantageous features of LMSM, this model is usually limited to the linear analysis. 3D FEM is considered as the most accurate and reliable model for simulating seismic behaviors of structures. Numerous studies conducted

* Corresponding author.
E-mail address: thlee@konkuk.ac.kr (T.-H. Lee).

https://doi.org/10.1016/j.net.2021.02.006
1738-5733/

seismic assessment and performance of NPP structures using 3D FEM [12–18]. However, 3D FEM requires a significant amount of CPU time and it is impractical to use this model for nonlinear analysis [10].

In addition to LMSM and 3D FEM, the shell elements can be used for modeling and analyzing the seismic response of NPP structures. Some studies utilized linear shell elements [19–22] to facilitate the numerical simulations. Besides, a multi-layer shell model (MLSM) considering the nonlinearity of materials was also applied to evaluate the behaviors of the NPP structures under internal pressures [23] and earthquakes [24–26]. Nevertheless, quantification of the difference between linear and nonlinear time-history analyses was also not investigated systematically.

Beam-truss element model (BTM) has been developed to model shear walls in conventional building structures [27–30]. So far, this modeling approach was not used in NPP structures, specifically for containment buildings. A systematic study on the efficiency of the aforesaid structural modeling schemes for seismic response evaluations of NPP structures has not been conducted yet.

Numerous studies have developed seismic fragility curves of containment buildings for reactors of early generations (e.g. CANDU, AP1000, Indian 700 MWe PHWR) using LMSM [2,3,31], 3D FEM [17,25,32–34]. However, a probabilistic vulnerability assessment of the RCB structure in APR1400 NPPs using nonlinear BTM is still not performed in the literature.

The aim of this study is to assess the efficiency of different finite element modeling schemes for seismic performance evaluations and fragility analyses of the containment building in the APR1400 NPP. Four structural modeling schemes, which are LMSM, solid-based finite element model (Solid FEM), MLSM, and BTM, are developed to simulate the seismic behaviors of the containment structure. Additionally, a full three-dimensional finite element model (full 3D FEM) is constructed to validate the aforementioned four modeling schemes. A set of input ground motions compatible with the US Nuclear Regulatory Commission (NRC) 1.60 design spectrum is generated to perform linear and nonlinear time-history analyses. Seismic responses of the RCB are measured in terms of floor response spectra and maximum floor displacements. Furthermore, a systematic assessment of the capability and efficiency of computational models is presented. Finally, seismic fragility curves of RCB are developed using a numerical model that is considered as an optimal one. The results of linear and nonlinear analyses are compared in terms of the fragility curves.

2. Numerical modeling

2.1. Description of RCB structure

The reinforced concrete (RC) containment building of the APR1400 NPP, which was developed by Korea Electric Power Corporation and Korea Hydro & Nuclear Power, was employed for numerical analyses in this study. The reactor containment cylinder has a 23.5 m radius, 54 m height, and 1.22 m thickness. The radius of the dome is 23.2 m, the average thickness is 1.07 m. Fig. 1 shows the elevation view of APR1400 where RCB is designated by the dash-lined rectangle and the dimensions of RCB as well as reinforcement details.

2.2. Lumped-mass stick model (LMSM)

The containment building is one of the largest structures in NPPs and finite element analyses with conventional continuum elements are impractically expensive. Therefore, to reduce the calculation efforts in simulations, a simplified numerical model, namely lumped-mass stick model (LMSM), has been commonly used in seismic analyses of NPP structures. In this study, LMSM of the RCB structure was developed using SAP2000 [35], a commercial structural analysis program. Concentrated masses and equivalent section properties were calculated based on the designed cross sections of the structure. RCB was modeled by elastic beam elements and lumped masses were assigned to associated nodes. The structure was divided into 14 elements, in which the length of each element was determined considering the variation of the stiffness of RCB and the connections to the internal structure and other equipment. The model is assumed to be fixed at the base. Fig. 2(a) shows the LMSM of RCB in SAP2000. The nodal masses and structural properties of RCB in LMSM are shown in Table 1.

2.3. Solid-based finite element model (solid FEM)

The three-dimensional FEM using solid elements is known as one of the most accurate models, and it is normally used to validate the simplified approach (i.e. LMSM). In this study, a solid FEM is constructed by ANSYS [36], a commercial structural analysis program and popular in the nuclear engineering community, as shown in Fig. 2(b). It is assumed that the base of the structure was fixed to the ground. We use an isotropic elastic material with Young's modulus of 30,000 MPa, Poisson's ratio of 0.17, and a density of 24.0 kN/m^3 to assign the structural model. A mesh convergence test is conducted to finalize the model with 13,571 elements. It should be noted that with this modeling scheme, the structure's behavior is completely limited within the linear elastic range. This kind of modeling has been widely applied in seismic performance analysis of NPP structures [9,10,13].

2.4. Multi-layer shell element model (MLSM)

A numerical model of RCB is developed using smeared multi-layer shell elements available in SAP2000 [35], as shown in Fig. 2(c). A shell element is divided into several layers with different thicknesses. Each layer represents a specific material, in which reinforcement and concrete layers are assumed to be perfectly bonded to each other, as shown in Fig. 3. Material properties including the nonlinearity of the material are assigned to corresponding layers. The multi-layer shell element was originally derived based on the principles of composite material mechanics. This kind of element can simulate the interaction between in-plane and out-of-plane responses as well as the in-plane flexural-shear behaviors of RC walls [37,38].

To set up MLSM, design details of reinforcing bars and concrete need to be pre-defined, as well as material properties. Thanks to the theoretical background of MLSM, it is expected to simulate nonlinear behaviors of a wall-type structure accurately. Since this numerical model significantly reduces the degrees of freedom compared to that of the Solid FEM approach, the computational cost is expected to be less high. In other words, MLSM can be a promising approach for analyzing larger structures like RCB.

2.5. Beam-truss element model (BTM)

In addition to LMSM, Solid FEM, and MLSM, a simplified but effective model, namely beam-truss element model (BTM), is developed in this study. This modeling approach discretizes the continuum RC wall into a combination of conventional beam and truss elements [27,28]. Since LMSM is the most simplified approach for modeling the structure, it purely simulates the seismic behavior in the elasticity. Additionally, full 3D FEM requires a very time-consuming calculation, specifically in nonlinear dynamic analyses. Therefore, BTM is developed to overcome aforesaid limitations. There are two advantages of using BTM. The first one is the

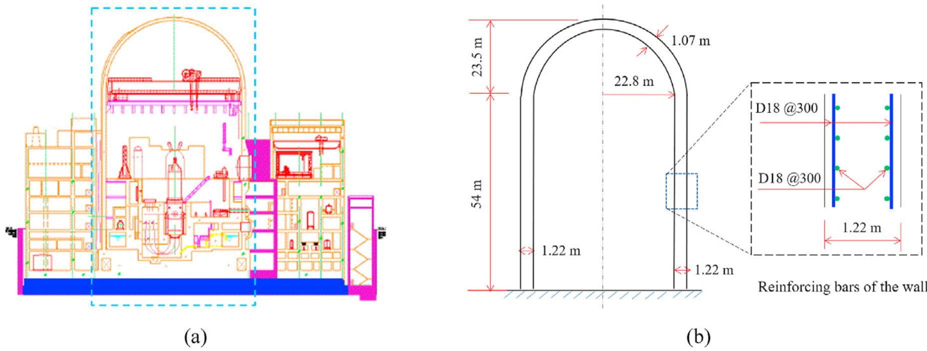

Fig. 1. APR1400: (a) elevation view and (b) dimensions of the RCB structure.

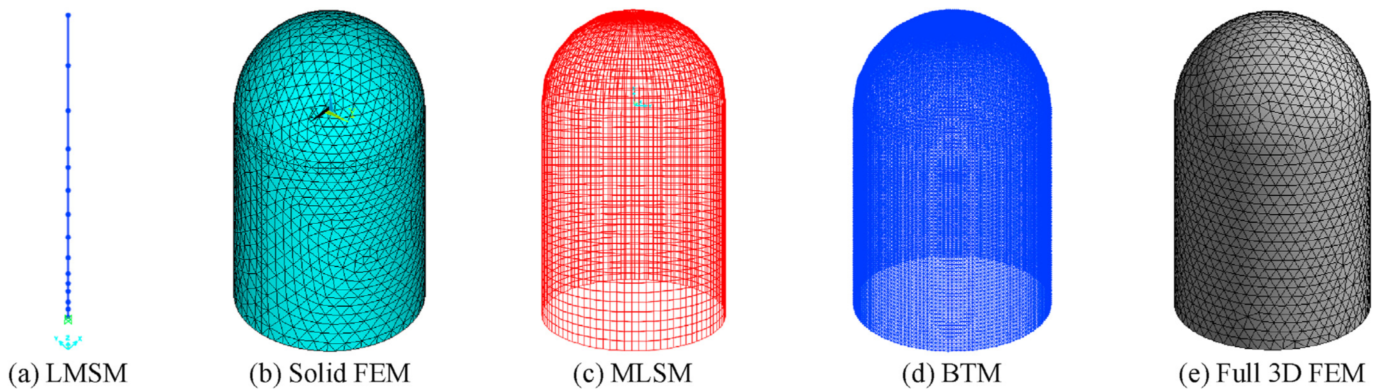

Fig. 2. Different numerical models of RCB.

Table 1
Structural properties of the RCB in LMSM.

Node	Height from base-mat (m)	Nodal mass (ton)	Area (m^2)	Moment of inertia (m^4)	Shear area (m^2)	Torsional inertia (m^4)
1	16.76	87.07	202.90	56299.85	101.45	112634.22
2	20.27	166.52	202.90	56299.85	101.45	112634.22
3	23.46	185.42	202.90	56299.85	101.45	112634.22
4	27.73	189.29	202.90	56299.85	101.45	112634.22
5	31.09	170.39	202.90	56299.85	101.45	112634.22
6	34.59	234.68	202.90	56299.85	101.45	112634.22
7	40.53	314.15	202.90	56299.85	101.45	112634.22
8	47.24	333.05	202.90	56299.85	101.45	112634.22
9	53.94	318.02	202.90	56299.85	101.45	112634.22
10	60.65	310.43	202.90	56299.85	101.45	112634.22
11	66.44	376.80	202.90	56299.85	101.45	112634.22
12	70.56	279.92	179.76	47591.20	89.89	95199.65
13	78.63	355.52	179.76	35861.70	89.89	71732.03
14	86.72	352.09	166.11	12825.63	83.03	25651.25
15	94.64	147.80				

simplicity of the model. Beam and truss elements are much easier to model a structure than conventional continuum elements. The second advantage is that it is possible to simulate the nonlinear behavior of a large structure with BTM while it is impractical with conventional continuum elements.

The dimensions of the beam and truss elements depend on the size of the panel (i.e. mesh size), which is determined using the sensitivity analysis. In this study, the length of the horizontal and vertical elements is set to 1.0 m after performing a mesh convergence test. Meanwhile, the width of those beam elements is equal to the thickness of the wall, i.e., 1.22 m, and the height of the beams is set to the size of the panels. Moreover, the width of the diagonal truss elements (b) is the product of the length of the panel (a) and $\sin(\theta_d)$, in which θ_d is the angle between the diagonal and the horizontal elements, expressed as

$$b = a \times \sin(\theta_d) \quad (1)$$

BTM is constructed in OpenSees [39], an open platform for earthquake engineering simulation, as shown in Fig. 4. The model comprises of the vertical and horizontal beam and diagonal truss elements. The vertical and horizontal beam elements consider the integration of concrete and reinforcements. Meanwhile, the diagonal truss elements represent the behavior of pure concrete. This modeling approach is adopted from the study of Lu and Panagiotou [27]. Fig. 5 shows the schematic modeling of the RCB wall using

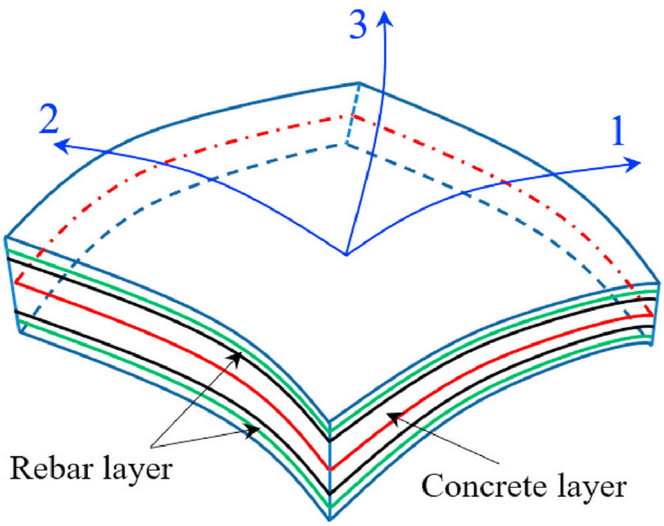

Fig. 3. Illustration of MLSM.

BTM. Nonlinear material models are adopted, i.e. *concrete02* [40] and *steel02* models [41] are applied for concrete and reinforcing bars, respectively. To accommodate the nonlinear behavior of beam elements, the *forceBeamColumn* elements with fiber sections are employed. The *corotTruss* element is used to construct the diagonal truss elements accounting for nonlinear properties of the concrete section.

2.6. Full three-dimensional finite element model (full 3D FEM)

A full 3D FEM, which comprises of details of reinforcing bars and concrete, is one of the most accurate approaches in the numerical modeling of structures. We develop this model in ANSYS [36] for the sake of verification of the proposed structural models earlier, as shown in Fig. 2(e). To construct full 3D FEM, the *solid187* element is used for concrete, the *beam189* element is applied for reinforcing bars, and the *conta174* is utilized to model the contact element between the concrete and reinforcing bars. Since a nonlinear time-history analysis of a full 3D FEM is impractical, we focus on the use of full 3D FEM with linear materials. We also used an isotropic elastic material for concrete with Young's modulus of 30,000 MPa, Poisson's ratio of 0.17, and a density of 24.0 kN/m^3, while Young's modulus of 2.0E+5 MPa, Poisson's ratio of 0.3, and a density of

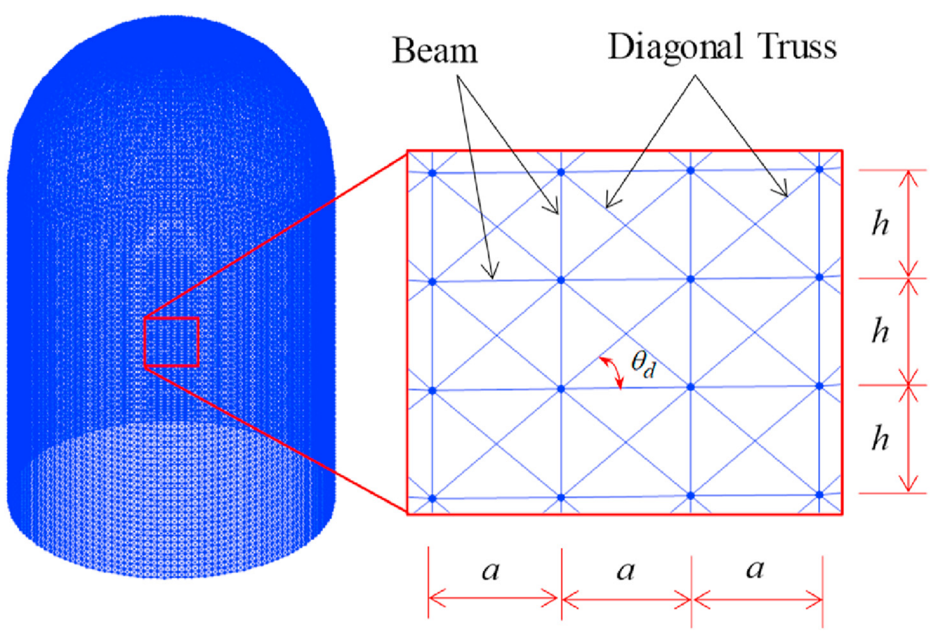

Fig. 4. Finite element model of RCB using BTM in OpenSees.

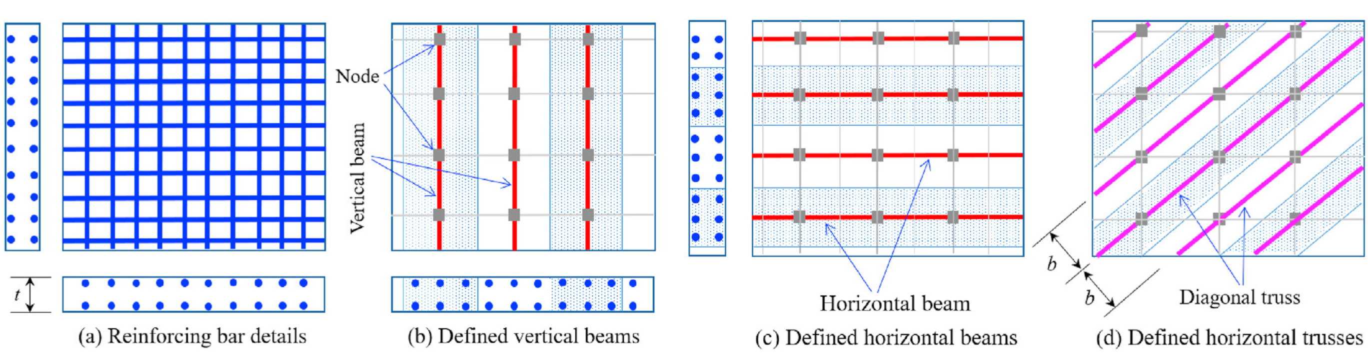

Fig. 5. Schematic numerical modeling of RCB wall using BTM.

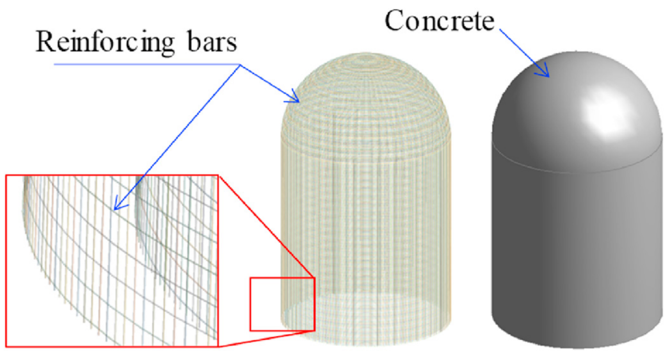

Fig. 6. Reinforcing bars and concrete part in full 3D FEM.

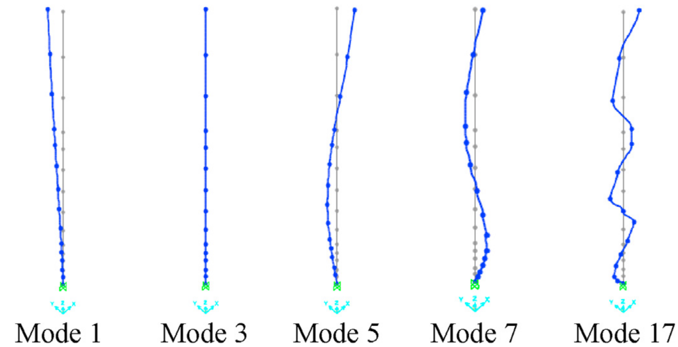

Fig. 7. Vibration modes of LMSM.

78.5 kN/m^3 are assigned to reinforcements. The model was meshed into 64,299 prism solid elements and 24,647 beam elements after conducting a mesh-sensitivity analysis. Fig. 6 shows the concrete part and reinforcing bars in full 3D FEM.

3. Eigenvalue analysis

For a fundamental validation of the proposed models, eigenvalue analyses are conducted, and results are discussed in this section. Fig. 7 shows the vibrational mode shapes of LMSM, while Fig. 8 shows those of Solid FEM, MLSM, BTM, and full 3D FEM. It is observed that for the fundamental modes (i.e. translations), the results of these models are highly comparable. The torsional vibration of LMSM is in mode 3, whereas it is fallen to mode 9 for other models. Since LMSM consists of conventional beam elements, it cannot simulate complex or local deformation modes such as a distortion of the cylinder, which can be simulated in Solid FEM, MSLM, BTM, and full 3D FEM. This phenomenon may lead to an inaccuracy in simulating dynamic responses of a structure for high-frequency earthquakes if LMSM is used. Table 2 presents the natural frequencies of the first 10 vibration modes of the four investigated models where frequencies of the comparable mode shape are in good agreement.

The results of MLSM and BTM are matched well with those of Solid FEM and full 3D FEM in all modal shapes and frequencies. It primarily implies that these models are capable of modeling dynamic responses of RCB. Furthermore, MLSM and BTM can be alternative approaches to solid and full FEMs in design practice or structural analysis of NPP structures.

4. Input ground motions

The APR1400 NPP structures have been seismically designed using the US Nuclear Regulatory Commission (NRC) 1.60 spectrum [42] with a PGA of 0.3 g at the safe shutdown earthquake level. A set of 11 ground motions are generated using the SeismoSignal program [43] to match the NRC 1.60 design spectrum for time history analyses, as shown in Fig. 9. The seed ground motion records are randomly selected from worldwide historic earthquakes provided in the PEER center database [44].

5. Seismic response analysis of RCB

5.1. Rayleigh damping

The Rayleigh damping model is commonly used in dynamic analyses [45], as expressed in the following form,

$$[C] = a[M] + b[K] \tag{2}$$

where $[C]$ is the damping matrix; $[M]$ and $[K]$ are the mass and stiffness matrices, respectively. a and b are the proportional damping coefficients, given by

$$a = \xi\frac{2\omega_i\omega_j}{\omega_i + \omega_j}; \quad b = \xi\frac{2}{\omega_i + \omega_j} \tag{3}$$

where ω_i and ω_j are the circular frequencies of the predominant modes, which are the first and the fifth modes for LMSM, while the first and the seventeenth modes for the other structural models, respectively; ξ is the damping ratio, set to 0.05 based on the suggestion of Park and Hofmayer [46].

5.2. Linear time-history analysis

Since the containment building is axisymmetric, dynamic analyses can be carried out by imposing ground motions in one horizontal direction [2,15,47]. Additionally, the difference of time-history responses of RCB subjected to the one- and three-dimensional ground motions is not significant, as pointed out in the study of Jin and Gong [47]. Therefore, we performed a series of linear time-history analyses in only the horizontal X-direction to obtain the seismic responses of RCB. It is noted that we apply the Newmark method with $\gamma = 0.5$ and $\beta = 0.25$, which yields the constant average acceleration method (i.e. middle point rule), for solving the equation of motion in dynamic analyses.

Floor response spectrum (FRS) is one of the most important outputs to evaluate the seismic performance of NPP structures. Also, there are numerous electrical, electronic, and mechanical components that are attached to the primary structures at different locations. Therefore, the seismic responses of the equipment and devices are normally evaluated by using FRS at such positions as input excitations. FRS of Solid FEM, MSLM, and BTM are computed at the intersection of the XZ plane and the containment model at the same height as LMSM. We obtained FRS at the top and mid-height of the structure for all analyses.

Fig. 10 compares the mean FRS′ of different numerical models at the top and mid-height of RCB. The FRS are mostly amplified at the fundamental frequency of RCB (i.e. approximately 4.0 Hz) for the top node. However, at the mid-height (i.e. middle node), FRS' are additionally amplified at a higher frequency, i.e. approximately 12.0 Hz. This behavior is attributed to the reason that the middle elevation of RCB is predominantly affected by higher modes. In this case, it is the second predominant mode that amplified the mid-height responses. Moreover, it is observed that the results of different numerical models are very comparable. This highlights that LMSM can well estimate linear floor responses of the structure. In addition to the common models such as LMSM and Solid FEM, MLSM and BTM can be good options for performing linear time-

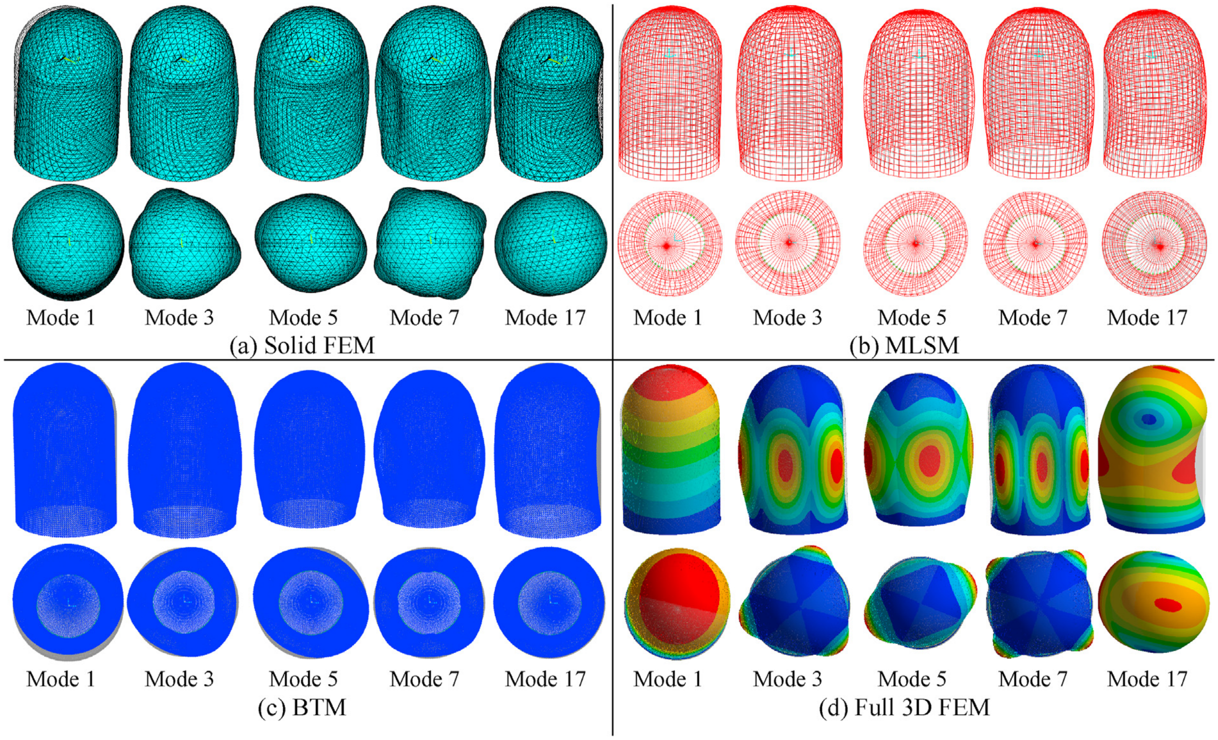

Fig. 8. Vibration modes of Solid FEM, MLSM, BTM, and Full 3D FEM.

Table 2
Natural frequencies (Hz) of the structure considering different numerical models.

Mode	LMSM	Solid FEM	MLSM	BTM	Full 3D FEM
1	3.85	3.97	4.01	3.99	3.92
2	3.85	3.97	4.01	3.99	3.92
3	8.37*	5.39	5.28	5.90	5.75
4	11.60	5.39	5.28	5.90	5.77
5	11.63**	6.35	6.19	6.16	6.55
6	11.63	6.35	6.19	6.16	6.55
7	21.96	6.82	6.62	7.58	6.93
8	21.96	6.82	6.62	7.58	6.93
9	24.20	8.50*	8.72*	8.81*	8.69*
17	40.31	11.85**	11.54**	11.93**	11.71**

Note: (*) is for the torsional mode; (**) is for the haft-cycle translational mode.

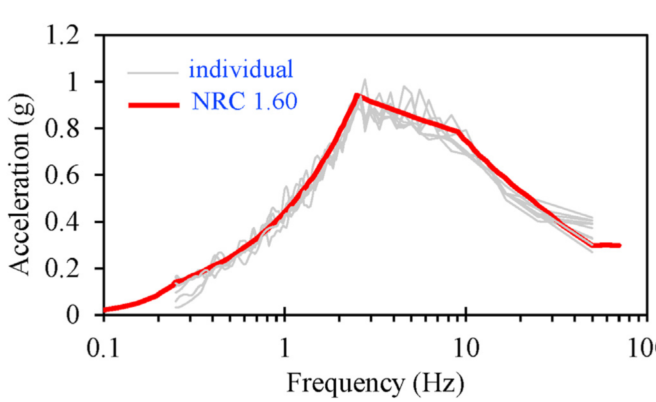

Fig. 9. Response spectra of input ground motions.

history analyses of NPP structures.

5.3. Nonlinear time-history analysis

The direct integration method is applied to perform nonlinear time-history analyses for the NPP structure. Similar to linear analyses, all the input motions are imposed in the horizontal X-direction for obtaining the seismic responses of RCB. The nonlinear analyses are carried out using MLSM and BTM since these models are less time-consuming than a full 3D FEM. A verification of nonlinear MLSM and BTM is performed by comparing their FRS with those of full 3D FEM, as shown in Fig. 11.

Mean nonlinear FRS of RCB using MLSM and BTM are compared in Fig. 12. It is observed that the spectral accelerations at the top node are amplified at the fundamental frequency of RCB, i.e. approximately 4.0 Hz. However, the spectral accelerations are additionally amplified at a higher frequency approximately 8.0 Hz at the mid-height of RCB (i.e. middle node). The comparison results demonstrate that a good agreement in FRS is achieved from MLSM and BTM.

Fig. 13 compares the mean linear and nonlinear FRS' between linear and nonlinear analyses. For the top node, spectral accelerations obtained from nonlinear analyses are slightly lower than those of linear analyses. It is because of the occurrence of concrete cracking at the bottom of the structure, leading to a reduction of the structural stiffness. A similar observation of the structural response can be found in studies elsewhere [15,17,18]. This also causes larger lateral displacements for nonlinear analyses compared to linear analyses, as shown in Fig. 14.

In the probabilistic seismic risk assessment, the probability of failure of NPP structures and components has to be evaluated at a wide range of seismic intensity measures. For that, we need to perform nonlinear analyses of RCB with an increment of PGA. Fig. 15 shows FRS with respect to various PGA levels at the top and mid-height of RCB. At a lower PGA, i.e. 0.3 g, the difference of FRS obtained from linear and nonlinear analyses is not significant. However, the discrepancy is getting larger as PGA increased to 0.6 g and

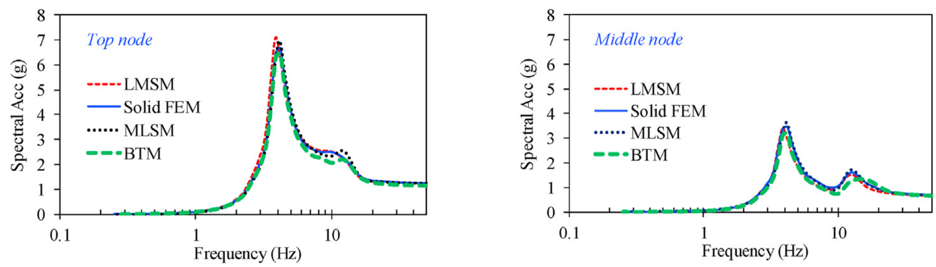

Fig. 10. Comparison of mean linear FRS of RCB between different models.

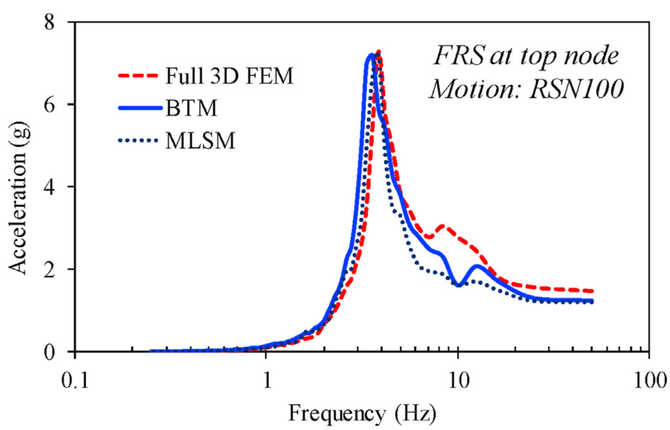

Fig. 11. Comparison of nonlinear FRS between MLSM, BTM, and Full 3D FEM.

1.0 g. Overall, spectral accelerations of linear FRS′ are larger than those of nonlinear FRS'. The shaking energy of the earthquake is absorbed as the structure suffers from the cracking of the concrete and the yielding of the reinforcements, and consequently, the floor accelerations are reduced. It is again to emphasize that the influence of the nonlinear analysis on seismic responses of RCB is pronounced since the linear analysis can lead to underestimate the structural displacements and overestimate the structural accelerations.

5.4. *Efficiency assessment of structural modeling schemes*

Quantitative and qualitative comparisons between proposed numerical models are presented to systematically assess the efficiency of different structural modeling schemes. Table 3 shows the computational time for linear and nonlinear dynamic analyses under an arbitrarily selected ground motion time history, i.e. the one recorded in the 1940 El Centro earthquake. It is seen that LMSM spends the shortest running time in the linear analysis, followed by BTM and MLSM. The longest CPU times are required for full 3D FEM and Solid FEM, which are 8400 and 400 times longer than that of LMSM, and 1260 and 60 times longer than that of BTM, respectively. These imply that LMSM, BTM, and MLSM can be good options for performing linear time-history analyses of NPP structures.

Nonlinear analyses are performed only by MLSM and BTM, since LMSM is a very simple approach, Solid FEM is incapable of simulating nonlinear behavior, and full 3D FEM requires an impractically long CPU time (approximately 28 days) and large computational storage. Thus, full 3D FEM is not recommended for nonlinear dynamic analyses in practical designs and vulnerability assessments of RCB structures. From Table 3, it is observed that running time in BTM is 5 times shorter than that using MLSM. This emphasizes that BTM can be a good selection for evaluating nonlinear time-history analyses of RCB structure.

Table 4 presents qualitative capability assessments of proposed numerical modeling schemes based on various criteria such as modeling effort, analysis method, computation time, observed response, storage, and cost. LMSM is a simple, fast running, and good model for linear analyses but it is incapable of simulating nonlinear responses. Solid FEM is simple to build a model and good at simulating global and local responses, but it is computationally expensive and limited to linear analyses. It should be noted that the global response term describes the floor responses or internal forces, while the local response represents the detailed simulation results such as stresses, strains, or cracking. Full 3D FEM is excellent in simulating global and local nonlinear behaviors, however, it requires a complicated modeling technique and an extremely long CPU time. Therefore, the evaluations of the global and local responses for full 3D FEM are focused only on linear analyses. Based on the given assessments, BTM is considered as the optimal structural modeling scheme for mostly satisfying all the mentioned criteria even if the local response capacity is still limited. MLSM might be the second best choice for evaluating seismic performances of RCB structures.

6. Fragility analysis

The fragility curve is a practical tool to assess the probabilistic vulnerability of structures subjected to seismic loadings. This study develops the fragility curves of RCB for different damage states

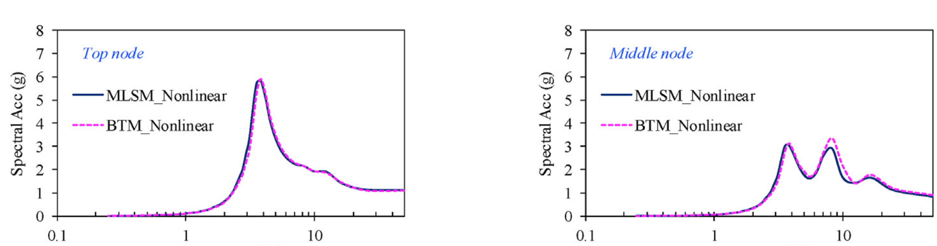

Fig. 12. Mean nonlinear FRS of RCB by MLSM and BTM.

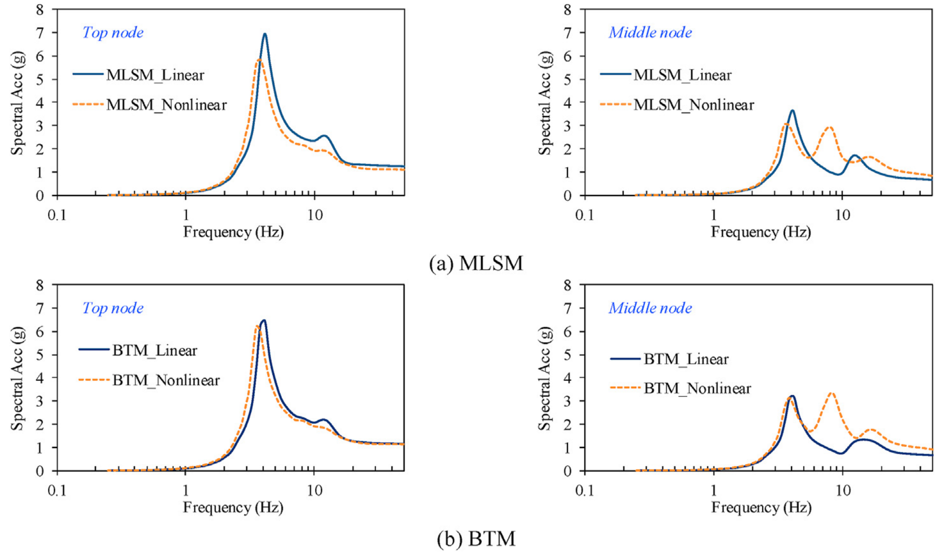

Fig. 13. Mean linear and nonlinear FRS' by MLSM and BTM.

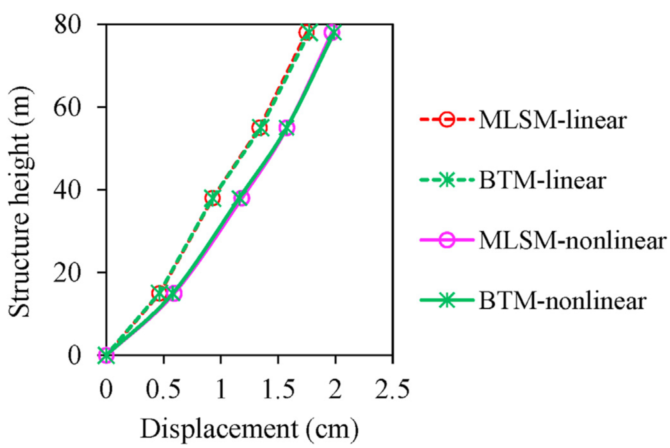

Fig. 14. Comparison of displacements between linear and nonlinear analyses.

using the optimal BTM scheme, time-history analysis, and maximum likelihood estimation. Both linear and nonlinear incremental dynamic analyses are performed to obtain the seismic behaviors of RCB with a variation of earthquake intensities.

6.1. Incremental dynamic analysis

A series of linear and nonlinear incremental dynamic analyses (IDA) are performed using BTM of RCB with a wide range of PGA up to 1.5 g. Fig. 16 shows the maximum displacements and accelerations at the top of RCB with respect to PGA in linear and nonlinear dynamic analyses. It can be found that the displacements in nonlinear analyses are larger than those in linear analyses and the gap is getting bigger as PGA increased, as shown in Fig. 16(a). In contrast, the acceleration responses are smaller for nonlinear analyses than those for linear analyses, as shown in Fig. 16(b). The reason can be attributed that the structure suffers from material

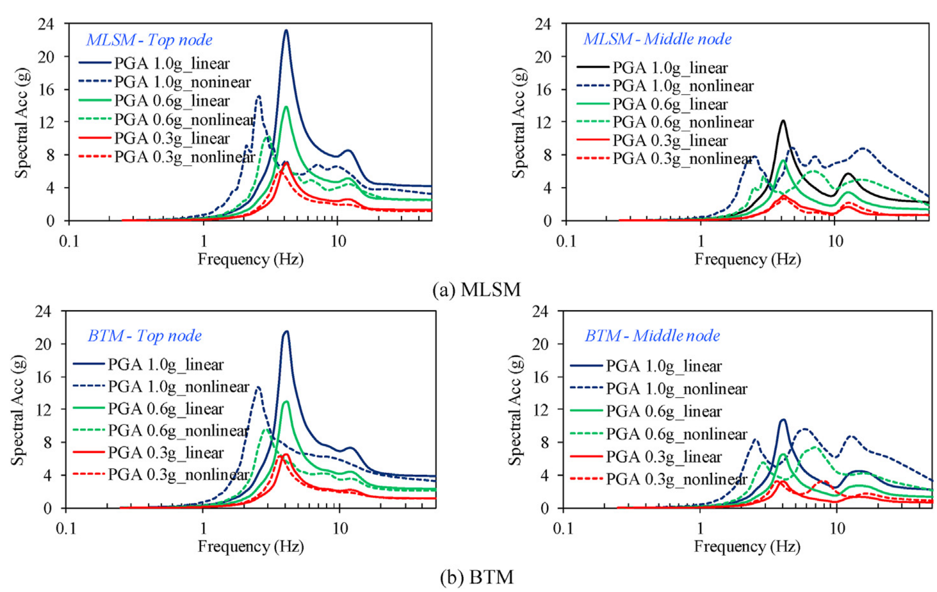

Fig. 15. FRS of RCB for various PGA levels.

Table 3
Computational times for time-history analyses of different numerical models under the 1940 El Centro earthquake (unit: mins).

Computer system	Analysis method	LMSM	Solid FEM	MLSM	BTM	Full 3D FEM
Intel Xeon(R) Platinum 8160 CPU @2.10 GHz,	Linear	0.3	120	9.0	2.0	2520
RAM 96 GB	Nonlinear	N.A.	N.A.	7560	1500	39,600

Table 4
Capability and applicable assessment of various models.

Criteria	LMSM	Solid FEM	MLSM	BTM	Full 3D FEM
Modeling effort	Quick	Quick	Quick	Moderate	Long
Linear computation time	Fast	Moderate	Fast	Fast	Moderate
Nonlinear computation time	N.A.	N.A.	Long	Moderate	Extremely long
Global response	Good	Good	Good	Good	Good
Local response	N.A.	Moderate	Moderate	Limited	Very good
Storage size	Small	Medium	Medium	Small	Very large
Cost	Free or Reasonable	Expensive	Free or Reasonable	Free or Reasonable	Expensive

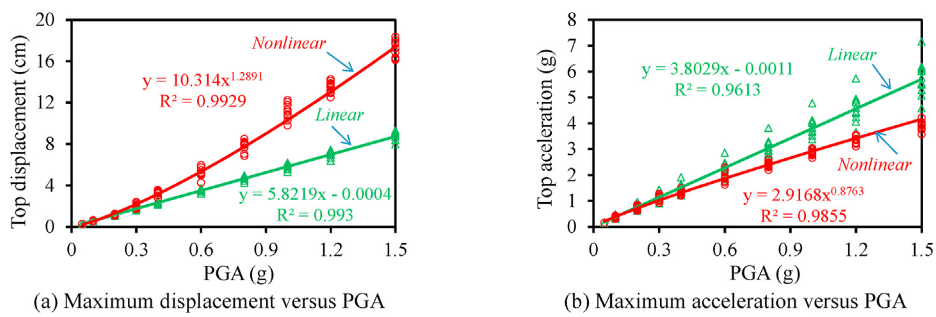

Fig. 16. Increment dynamic responses of RCB.

damage as earthquake intensity increased, which caused a reduction of the global stiffness, and accordingly, the horizontal displacement is increased while the acceleration is decreased. We are showing herein the acceleration response because it is the critical input to evaluate the seismic behaviors of the secondary systems such as mechanical equipment, electrical devices, or pipelines. Fig. 16 delivers an important message that a linear analysis may underestimate floor displacements while it may overestimate floor accelerations of RCB.

6.2. Definition of damage states

To develop fragility curves, damage states should be defined. There are proposed definitions of damage states for shear walls in buildings [48] and nuclear facilities [49]. However, since RCB is a special structure with combining a dome and cylinder, it is obviously different from other conventional RC wall structures. A specific guideline for defining damage states of curved RC walls is not proposed yet. Therefore, damage states and corresponding damage indices should be defined based on the capacity of the structure itself rather than adopting the existing references, which were proposed for common flat shear walls. In this study, a pushover analysis is performed to obtain the capacity curve and identify the cumulative damages of the structure, as shown in Fig. 17.

The top lateral displacement is a critical response of the containment building since the fundamental vibrational mode is a simple cantilever mode [2,17]. A damage index is specified in terms of the top displacement and the drift ratio which corresponds to damage levels of RCB. Four damage states, which are minor (i.e. concrete cracking, referred as DS1), moderate (i.e. rebar yielding, referred as DS2), extensive (i.e. extensive cracking and yielding at the bottom, referred as DS3), and collapse (i.e. crushing, referred as DS4), are defined based on the pushover analysis. In particular, DS3 and DS4 are defined at the states corresponding to the ductility of 4.8 and 7.2, respectively. This approach is also consistent with studies elsewhere [17]. Table 5 shows the proposed DSs and corresponding damage indices.

6.3. Fragility curves

A procedure based on the maximum likelihood estimation (MLE) proposed by Shinozuka et al. [50] is employed to generate fragility curves in this study. The fragility function is expressed in terms of log-normal cumulative distribution function, given by

$$P(\mathrm{IM}) = \Phi\left[\frac{\ln(\mathrm{IM}/\mu)}{\beta}\right] \quad (4)$$

where IM is the earthquake intensity measure, i.e. PGA in this study; $\Phi[-]$ is the standard normal cumulative distribution function; μ and β are the median and the standard deviation of ln(IM), respectively. The standard deviation (β) is a combination of two main uncertainty sources: epistemic uncertainty due to numerical modeling (β_U) and randomness in selected ground motions (β_R), defined by Eq. (5).

$$\beta = \sqrt{\beta_U^2 + \beta_R^2} \quad (5)$$

The β_R value is estimated by MLE, while β_U is set to 0.32 according to the suggestion of Ozaki et al. [51] and other applications [2,47].

Fig. 18(a) shows fragility curves of RCB based on linear and

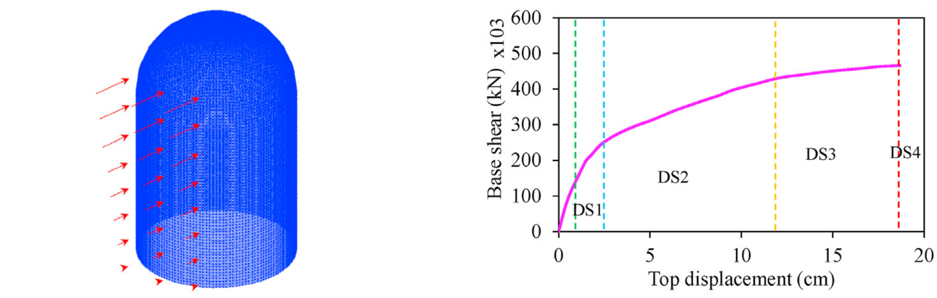

(a) Applied loads in the pushover analysis

(b) The base shear-top displacement curve

Fig. 17. Pushover analysis of RCB.

Table 5
Defined limit states and drift limits based on pushover analysis.

Damage state	Displacement (cm)	Drift (%)	Description
DS1 (Minor)	0.75	0.01	Concrete cracking
DS2 (Moderate)	2.5	0.03	Rebar yielding
DS3 (Extensive)	12.0	0.15	Extensive cracking & yielding at the bottom
DS4 (Collapse)	18.0	0.23	Concrete crushing

nonlinear analyses for defined damage states. It is obvious that the probability of failure for nonlinear analyses is larger than that of linear analyses at a given PGA and the difference is large for DS3 and DS4, in particular. It indicates that a seismic safety evaluation of the RCB structure based on a linear analysis may underestimate its actual vulnerability. Therefore, we recommend using the nonlinear dynamic analysis method in evaluating seismic performances and assessing the vulnerability of NPP structures. It should be noted that the developed fragility curves may give a conservative estimation since the influence of prestressing tendons on the behavior of the structure is not considered in this study. Fig. 18(b) shows a comparison of fragility curves with and without uncertainties in numerical modeling (β_U). It is observed that the presence of β_U has a moderate influence on the probability of failure of the structure. Without consideration of this uncertainty source may estimate a smaller posibility of damage under the median level.

Comparisons of the proposed fragility curves from nonlinear analyses and the results of Bao et al. [17] are shown in Fig. 18(c) and (d). The fragility curves of Bao et al. [17] were developed for a similar containment structure using a full 3D FEM in ABAQUS. The RC containment structure of Bao et al. [17] is in a Chinese NPP with 63.26 m height and 39.93 m diameter, which is smaller than the RCB in APR1400 NPPs with 77.5 m height and 48 m diameter. Four limit states (i.e. damage states) were defined as concrete cracking (LS1), steel yielding (LS2), concrete crushing (LS3), and near ultimate (LS4) [17]. The developed fragility curves without β_U in this study are overall comparable to those of the existing work except for DS2. However, there is a moderate difference between those curves as shown in Fig. 18(d) when the uncertainty β_U is included. An uncertainty in the structural modeling was not included in the fragility curves of the reference work. The comparison implies that BTM is capable of performing seismic fragility analyses of RCB structures.

The seismic capacity of NPP structures in the seismic

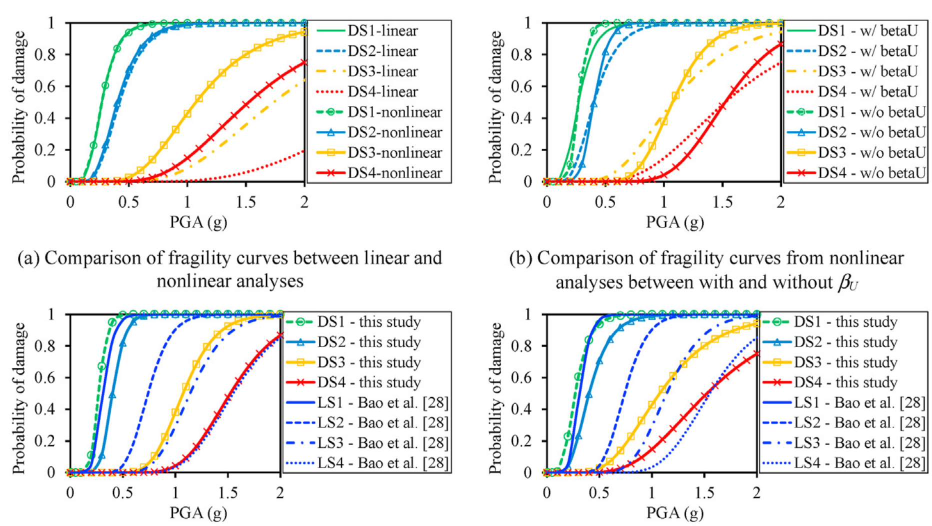

(a) Comparison of fragility curves between linear and nonlinear analyses

(b) Comparison of fragility curves from nonlinear analyses between with and without β_U

(c) Comparison with results of Bao et al. [28] without β_U

(d) Comparison with results of Bao et al. [28] with β_U

Fig. 18. Fragility curves of RCB in this study and comparison with the published result.

probabilistic risk analysis (SPRA) is normally expressed either using the fragility curves or high confidence of low probability of failure (HCLPF) capacity. The HCLPF value in the SPRA is normally defined as 95% confidence of less than 5% probability of failure. In this study, HCLPF values for four damage states, DS1, DS2, DS3, DS4, are 0.17 g, 0.26 g, 0.6 g, and 0.81 g, respectively.

7. Conclusions

Seismic performances of the RCB structure in APR1400 NPPs were evaluated based on a series of time-history analyses considering the efficiency of various structural modeling schemes. Four numerical models, which are LMSM, Solid FEM, MLSM, and BTM were developed for seismic performance evaluations. The influence of nonlinear structural modeling on FRS and fragility analyses are also assessed in this study. The following conclusions are drawn based on the numerical analysis results.

(1) LMSM is as good as Solid FEM, MLSM, and BTM in evaluating the linear time-history responses of RCB under the design earthquake excitations.
(2) FRS based on the linear and nonlinear analyses are different even under the design earthquake level. The discrepancy becomes larger as PGA increased. The linear analysis underestimates floor displacements and overestimates floor accelerations. It highlights the necessity of considering nonlinear modeling in designs and analyses for NPP structures.
(3) MLSM and BTM can be practical tools for accurate nonlinear analyses of RCB considering the CPU time and the modeling efforts.
(4) In terms of the modeling efforts, CPU time, and accuracy of simulating responses, BTM is an optimal model for evaluating the nonlinear seismic performance of NPP structures.
(5) The probability of damage is smaller for linear analysis compared with those for nonlinear analysis at a given intensity measure. Therefore, a nonlinear analysis approach should be employed for assessing the vulnerability of NPP structures.

Declaration of competing interest

The authors declare that they have no known competing financial interests or personal relationships that could have appeared to influence the work reported in this paper.

Acknowledgement

This paper was supported by Konkuk University Researcher Fund in 2020. The authors also acknowledge the fund of the Korea Institute of Energy Technology Evaluation and Planning (KETEP) and the Ministry of Trade, Industry & Energy (MOTIE) of the Republic of Korea (No. 20201510100020).

References

[1] V. Varma, G.R. Reddy, K.K. Vaze, H.S. Kushwaha, Simplified approach for seismic analysis of structures, Int. J. Struct. Stabil. Dynam. 2 (2002) 207–225, 02.
[2] I.K. Choi, Y.S. Choun, S.M. Ahn, J.M. Seo, Probabilistic seismic risk analysis of CANDU containment structure for near-fault earthquakes, Nucl. Eng. Des. 238 (6) (2008) 1382–1391.
[3] A. Ali, N.A. Hayah, D. Kim, S.G. Cho, Probabilistic seismic assessment of base-isolated NPPs subjected to strong ground motions of Tohoku earthquake, Nuclear Engineering and Technology 46 (5) (2014) 699–706.
[4] I. Zentner, Numerical computation of fragility curves for NPP equipment, Nucl. Eng. Des. 240 (6) (2010) 1614–1621.
[5] Y.N. Huang, A.S. Whittaker, N. Luco, A probabilistic seismic risk assessment procedure for nuclear power plants:(I) Methodology, Nucl. Eng. Des. 241 (9) (2011) 3996–4003.
[6] D.D. Nguyen, B. Thusa, T.S. Han, T.H. Lee, Identifying significant earthquake intensity measures for evaluating seismic damage and fragility of nuclear power plant structures, Nuclear Engineering and Technology 52 (1) (2020) 192–205.
[7] J.W. Jung, H.W. Jang, J.H. Kim, J.W. Hong, Effect of second hardening on floor response spectrum of a base-isolated nuclear power plant, Nucl. Eng. Des. 322 (2017) 138–147.
[8] S.G. Cho, D. Kim, S. Chaudhary, A simplified model for nonlinear seismic response analysis of equipment cabinets in nuclear power plants, Nucl. Eng. Des. 241 (8) (2011) 2750–2757.
[9] J.B. Park, N.C. Park, S.J. Lee, Y.P. Park, Y. Choi, Seismic analysis of the APR1400 nuclear reactor system using a verified beam element model, Nucl. Eng. Des. 313 (2017) 108–117.
[10] H. Lee, Y.C. Ou, H. Roh, J.S. Lee, Simplified model and seismic response of integrated nuclear containment system based on frequency adaptive lumped-mass stick modeling approach, KSCE Journal of Civil Engineering 19 (6) (2015) 1757–1766.
[11] Y.C. Ou, I. Hashlamon, W. Kim, H. Roh, Development of basic technique to improve seismic response accuracy of tributary area-based lumped-mass stick models, Earthq. Eng. Eng. Vib. 18 (1) (2019) 113–127.
[12] L. Tunon-Sanjur, R.S. Orr, S. Tinic, D.P. Ruiz, Finite element modeling of the AP1000 nuclear island for seismic analyses at generic soil and rock sites, Nucl. Eng. Des. 237 (12–13) (2007) 1474–1485.
[13] A. Nour, A. Cherfaoui, V. Gocevski, P. Léger, Probabilistic seismic safety assessment of a CANDU 6 nuclear power plant including ambient vibration tests: case study, Nucl. Eng. Des. 304 (2016) 125–138.
[14] A.G. Sextos, G.D. Manolis, A. Athanasiou, N. Ioannidis, Seismically induced uplift effects on nuclear power plants. Part 1: containment building rocking spectra, Nucl. Eng. Des. 318 (2017) 276–287.
[15] C.H. Zhai, X. Bao, Z. Zheng, X.Y. Wang, Impact of aftershocks on a post-mainshock damaged containment structure considering duration, Soil Dynam. Earthq. Eng. 115 (2018) 129–141.
[16] X. Huang, O.S. Kwon, E. Bentz, J. Tcherner, Method for evaluation of concrete containment structure subjected to earthquake excitation and internal pressure increase, Earthq. Eng. Struct. Dynam. 47 (6) (2018) 1544–1565.
[17] X. Bao, M.H. Zhang, C.H. Zhai, Fragility analysis of a containment structure under far-fault and near-fault seismic sequences considering post-mainshock damage states, Eng. Struct. 198 (2019) 109511.
[18] D. Wang, C. Wu, Y. Zhang, Z. Ding, W. Chen, Elastic-plastic behavior of AP1000 nuclear island structure under mainshock-aftershock sequences, Ann. Nucl. Energy 123 (2019) 1–17.
[19] S. De Grandis, M. Domaneschi, F. Perotti, A numerical procedure for computing the fragility of NPP components under random seismic excitation, Nucl. Eng. Des. 239 (11) (2009) 2491–2499.
[20] V. Jussila, Y. Li, L. Fülöp, Statistical analysis of the variation of floor vibrations in nuclear power plants subject to seismic loads, Nucl. Eng. Des. 309 (2016) 84–96.
[21] J. Hur, E. Althoff, H. Sezen, R. Denning, T. Aldemir, Seismic assessment and performance of nonstructural components affected by structural modeling, Nuclear Engineering and Technology 49 (2) (2017) 387–394.
[22] G. Dundulis, R. Kačianauskas, D. Markauskas, E. Stupak, S. Stupak, S. Šliaupa, Reanalysis of the floor response spectra of the ignalina nuclear power plant reactor building, Nucl. Eng. Des. 324 (2017) 260–268.
[23] H.P. Lee, Shell finite element of reinforced concrete for internal pressure analysis of nuclear containment building, Nucl. Eng. Des. 241 (2) (2011) 515–525.
[24] N. Nakamura, N. Yabushita, T. Suzuki, J. Yamada, N. Tsunashima, T. Nakano, Analyses of reactor building by 3D nonlinear FEM models considering base-mat uplift for simultaneous horizontal and vertical ground motions, Nucl. Eng. Des. 238 (12) (2008) 3551–3560.
[25] N. Nakamura, S. Akita, T. Suzuki, M. Koba, S. Nakamura, T. Nakano, Study of ultimate seismic response and fragility evaluation of nuclear power building using nonlinear three-dimensional finite element model, Nucl. Eng. Des. 240 (1) (2010) 166–180.
[26] W. Chao, The applicability study on the multi-layer shell element method in steel concrete structure of shield building, in: 2017 25th International Conference on Nuclear Engineering, American Society of Mechanical Engineers Digital Collection, 2017.
[27] Y. Lu, M. Panagiotou, I. Koutromanos, Three-dimensional beam-truss model for reinforced concrete walls and slabs—part 1: modeling approach, validation, and parametric study for individual reinforced concrete walls, Earthq. Eng. Struct. Dynam. 45 (9) (2016) 1495–1513.
[28] Y. Lu, M. Panagiotou, Three-dimensional beam—truss model for reinforced concrete walls and slabs—part 2: modeling approach and validation for slabs and coupled walls, Earthq. Eng. Struct. Dynam. 45 (11) (2016) 1707–1724.
[29] H. Park, T. Eom, Truss model for nonlinear analysis of RC members subject to cyclic loading, J. Struct. Eng. 133 (10) (2007) 1351–1363.
[30] M. Panagiotou, J.I. Restrepo, M. Schoettler, G. Kim, Nonlinear cyclic truss model for reinforced concrete walls, ACI Struct. J. 109 (2) (2012) 205.
[31] S.G. Cho, Y.H. Joe, Seismic fragility analyses of nuclear power plant structures based on the recorded earthquake data in Korea, Nucl. Eng. Des. 235 (17–19) (2005) 1867–1874.

[32] T.K. Mandal, S. Ghosh, N.N. Pujari, Seismic fragility analysis of a typical Indian PHWR containment: comparison of fragility models, Struct. Saf. 58 (2016) 11–19.
[33] C. Li, C. Zhai, S. Kunnath, D. Ji, Methodology for selection of the most damaging ground motions for nuclear power plant structures, Soil Dynam. Earthq. Eng. 116 (2019) 345–357.
[34] Z. Zheng, X. Pan, X. Bao, Seismic fragility of a typical containment under bidirectional earthquake excitations, KSCE Journal of Civil Engineering 22 (11) (2018) 4430–4444.
[35] Sap2000, C. S. I, Computers and structures Inc., Berkeley, CA, USA, 2013.
[36] Ansys, Inc, ANSYS Mechanical APDL Element Reference, 2019.
[37] Z.W. Miao, X.Z. Lu, J.J. Jiang, L.P. Ye, Nonlinear FE model for RC shear walls based on multi-layer shell element and microplane constitutive model, Computational Methods in Engineering and Science (2006) 21–23.
[38] X. Lu, L. Xie, H. Guan, Y. Huang, X. Lu, A shear wall element for nonlinear seismic analysis of super-tall buildings using OpenSees, Finite Elem. Anal. Des. 98 (2015) 14–25.
[39] S. Mazzoni, F. McKenna, M.H. Scott, G.L. Fenves, OpenSees Command Language Manual. Pacific Earthquake Engineering Research, PEER) Center, 2006, p. 264.
[40] D.C. Kent, R. Park, Flexural members with confined concrete, J. Struct. Div. 97 (7) (1971) 1969–1990.
[41] M. Menegotto, P.E. Pinto, Method of analysis for cyclically loaded reinforced concrete plane frames including changes in geometry and non-elastic behavior of elements under combined normal force and bending, in: IABSE Sym. Of Resist. and Ult. Deform. of Struct. Acted on by Well-Defined Repeat, Loads, Lisbon, Portugal, 1973.
[42] Nrc, US Nuclear Regulatory Commission 1.60: Design Response Spectra for Seismic Design of Nuclear Power Plants. Regulatory Guide 1.60, Revision 2, 2014. Rockville, Maryland, USA.
[43] SeismoSignal, A computer program for signal processing of strong-motion data. http://www.seismosoft.com, 2017.
[44] Peer center, PEER Ground Motion Database. Pacific Earthquake Engineering Research Center, University of California, Berkeley, CA, USA, 2020. http://ngawest2.berkeley.edu.
[45] A.K. Chopra, Dynamics of Structures: Theory and Applications to Earthquake Engineering, Prentice Hall. Inc., Upper Saddle River, NJ, USA, 1995.
[46] Y.J. Park, C.H. Hofmayer, Technical Guidelines for Aseismic Design of Nuclear Power Plants (No. NUREG/CR-6241), Nuclear Regulatory Commission, USA, 1994.
[47] S. Jin, J. Gong, Damage performance based seismic capacity and fragility analysis of existing concrete containment structure subjected to near fault ground motions, Nucl. Eng. Des. 360 (2020) 110478.
[48] Fema 356, Prestandard and Commentary for the Seismic Rehabilitation of Buildings in Rehabilitation Requirements, Federal Emergency Management Agency, Washington, DC, USA, 2000.
[49] Asce/Sei 43-05, Seismic Design Criteria for Structures, Systems, and Components in Nuclear Facilities, American Society of Civil Engineers, Reston, Virginia, USA, 2005.
[50] M. Shinozuka, M.Q. Feng, J. Lee, T. Naganuma, Statistical analysis of fragility curves, J. Eng. Mech. 126 (12) (2000) 1224–1231.
[51] M. Ozaki, A. Okazaki, K. Tomomoto, T. Iba, R. Satoh, H. Nanba, H. Seya, K. Moriyama, T. Ugata, Improved response factor methods for seismic fragility of reactor building, Nucl. Eng. Des. 185 (2–3) (1998) 277–291.